ospheric cooling calculations for Mars (*1*) and is between the present total moment release rates (*21*) for the moon (10^{22} dyne·cm/year) and the Earth (10^{29} dyne·cm/year), as would be expected from a simple comparison of the geologic and tectonic activity of the planets.

Our results in this paper are quite sensitive to poorly constrained assumptions of the distribution of seismicity (values for B and M_o*) and of the relative contribution of seismicity associated with surface faulting versus that attributable to the entire seismogenic lithosphere. Nevertheless, reasonable assumptions based on applicable data from the Earth and moon imply that Mars is a seismically active planet (Table 1, fourth column). For the total moment release rate for the entire lithosphere and the moment frequency distribution derived earlier, these estimates predict that about two marsquakes of moment $\geq 10^{23.5}$ dyne·cm, about a hundred marsquakes of moment $\geq 10^{20.5}$ dyne·cm, about a thousand marsquakes of moment $\geq 10^{19}$ dyne·cm, and tens of thousands of marsquakes of moment $\geq 10^{17}$ dyne·cm occur per year. The small size of Mars and a number of other factors support the argument that a marsquake equivalent to a body-wave event of magnitude 4 on Earth should be globally detectable by Apollo-class seismometers (*1*). If this statement is true, ~14 teleseismic events and more than a hundred equivalent magnitude 3 or greater earthquakes on Mars would be expected each year. Such events offer a promising prospect for seismological investigations on future missions to Mars.

REFERENCES AND NOTES

1. S. C. Solomon *et al.*, *Technical Report No. 91-02* (Lunar Planetary Institute, Houston, TX, 1991). See R. J. Phillips, *ibid.*, pp. 35–38, for lithosphere cooling calculations and E. A. Okal, *ibid.*, pp. 43–47, for expected seismometer response.
2. D. L. Anderson *et al.*, *J. Geophys. Res.* **82**, 4524 (1977); N. R. Goins and A. R. Lazarewicz, *Geophys. Res. Lett.* **6**, 368 (1979).
3. Y. Nakamura, *Proc. Lunar Planet. Sci. Conf.* 11, 1847 (1980).
4. K. L. Tanaka, M. P. Golombek, W. B. Banerdt, *J. Geophys. Res.* **96**, 15,617 (1991).
5. D. H. Scott and J. M. Dohm, *Proc. Lunar Planet. Sci. Conf.* **20**, 487 (1990).
6. Calibration of martian stratigraphy to two crater-absolute time scales is from K. L. Tanaka [*Proc. Lunar Planet. Sci. Conf.* 17, E139 (1986)]. First interval quoted in text here uses crater time scale of W. K. Hartmann *et al.* [in *Basaltic Volcanism on the Terrestrial Planets* (Pergamon, New York, 1981), pp. 1049–1127]. Second interval quoted in text uses crater time scale of G. Neukum and D. U. Wise [*Science* **194**, 1381 (1976)].
7. W. B. Banerdt, M. P. Golombek, K. L. Tanaka, in *Mars*, H. Keiffer, B. Jakosky, C. Snyder, Eds. (Univ. of Arizona Press, Tucson, in press).
8. P. A. Davis and M. P. Golombek, *J. Geophys. Res.* **95**, 14231 (1990).
9. K. L. Tanaka and P. A. Davis, *ibid.* **93**, 14893 (1988).
10. T. R. Watters and T. A. Maxwell, *Icarus* **56**, 278 (1983).
11. N. E. Witbeck, K. L. Tanaka, D. H. Scott, *U.S. Geol. Surv. Map I-2010* (1991).
12. J. B. Plescia, *J. Geophys. Res.* **96**, 18,883 (1991).
13. M. P. Golombek, J. B. Plescia, B. J. Franklin, *Proc. Lunar Planet. Sci. Conf.* **21**, 679 (1991).
14. J. Filson, T. Simkin, L. J. Leu, *J. Geophys. Res.* **78**, 8591 (1973).
15. P. J. Thomas, S. W. Squyres, M. H. Carr, *ibid.* **95**, 14 345 (1990).
16. P. J. Mouginis-Mark, *Proc. Lunar Planet. Sci. Conf.* **12B**, 1431 (1981); R. J. Pike, *ibid.* **9**, 3239 (1978).
17. E. A. Bergman, *Tectonophysics* **132**, 1 (1986); S. C. Solomon, catalog of 141 oceanic intraplate earthquakes, personal communication.
18. B. K. Lucchitta and J. A. Watkins, *Proc. Lunar Planet. Sci. Conf.* **9**, 3459 (1978).
19. S. C. Solomon and J. W. Head, *Rev. Geophys. Space Phys.* **18**, 104 (1980).
20. M. P. Golombek, *J. Geophys. Res.* **84**, 4657 (1979).
21. J. Oberst, *ibid.* **92**, 1397 (1987); N. R. Goins, A. M. Dainty, M. N. Toksoz, *ibid.* **86**, 378 (1981).

22. Supported by grants from the National Aeronautics and Space Administration Planetary Geology and Geophysics Program to the Jet Propulsion Laboratory, California Institute of Technology, and the U.S. Geological Survey. We thank S. Solomon, R. Phillips, and P. Lundgren for many helpful discussions and for preprints and data in advance of publication. We also thank T. Watters for use of a digitized data set of martian grabens and wrinkle ridges and P. Schenk for use of a computer code to determine the lengths of structures.

21 May 1992; accepted 26 August 1992

Relation Between Long-Term Trends of Oxygen-18 Isotope Composition of Precipitation and Climate

Kazimierz Rozanski, Luis Araguás-Araguás, Roberto Gonfiantini

Stable isotope ratios of oxygen ($^{18}O/^{16}O$) and hydrogen (D/H) in water have long been considered powerful indicators of paleoclimate. However, quantitative interpretation of isotope variations in terms of climate changes is hampered by a limited understanding of physical processes controlling the global isotope behavior. Analysis was conducted of time series of ^{18}O content ($\delta^{18}O$) of monthly precipitation and surface air temperature available through the International Atomic Energy Agency–World Meteorological Organization global network, "Isotopes in Precipitation." This study indicates that long-term changes of isotopic composition of precipitation over mid- and high-latitude regions during the past three decades closely followed long-term changes of surface air temperature with the average $\delta^{18}O$-temperature coefficient around 0.6 per mil per degree Celsius.

Current distribution patterns of deuterium (HDO) and oxygen-18 ($H_2{}^{18}O$) concentrations in meteoric waters (rain and snow) reveal a close relation among some climatically relevant meteorological parameters, such as surface air temperature or amount and isotopic composition of precipitation (*1–6*). These relations have been used in numerous studies to extract paleoclimatic information from records of isotopic composition of ancient precipitation preserved in polar ice cores (*7–12*), carbonate deposits in lakes (*13–15*), ground water (*16–18*), and tree cellulose (*19–21*). Whereas the link between isotope signature of precipitation and climate in polar regions is relatively well understood, this is much less the case in temperate and tropical areas. Doubts have often arisen as to whether spatial relations between isotopic composition of precipitation and climatic variables, derived for current conditions, can be used with confidence to interpret isotope records preserved in various environmental archives because they usually reflect long-term linkage between isotopic composition of precipitation and climate on a given area.

The global survey of oxygen and hydrogen isotope composition of monthly precipitation, initiated in 1961 by the International Atomic Energy Agency (IAEA) in cooperation with the World Meteorological Organization (WMO), provides an opportunity to study the link between isotopic composition of modern precipitation and present climatic conditions on a global scale (Fig. 1). The most important paleoclimatic application is an apparent relation between isotopic composition of precipitation and surface air temperature. Dansgaard (*2*), in his excellent review of the data gathered during the first 3 years of operation of the IAEA/WMO network, noticed that annual mean $\delta^{18}O$ of precipitation was closely related to annual mean surface air temperature for mid- and high northern latitude coastal stations (North Atlantic and Greenland); the slope of the linear fit to the data was 0.69 per mil per degree Celsius. This spatial relation can also be derived from simple models describing the evolution of isotopic composition of atmospheric waters at various stages of the global water cycle (*2, 3, 22–26*). The concept most often applied assumes that rain is formed in isotopic equilibrium with the vapor, at the temperature of the cloud base, and is immediately removed from the cloud (Rayleigh model). Because heavy water molecules ($H_2{}^{18}O$) are preferred in the

International Atomic Energy Agency, 1400-Vienna, Austria.

condensation process, the remaining cloud vapor is progressively depleted in ^{18}O. The theoretically derived slope of the $\delta^{18}O$-temperature relation varies between 0.72 and 0.52 per mil per degree Celsius between 0° and 20°C, respectively. These values are reached on the assumption that an isolated air mass undergoes isobaric cooling (*22, 23*).

Today, relatively long records of isotope and meteorological data are available for a number of stations in the IAEA/WMO network, in several cases going back three decades (*27*). Therefore, we used these records to reexamine the $\delta^{18}O$-temperature relation and to search for long-term trends in isotope records, in connection with the postulated global warming over the past decade. The selection of stations for analysis was guided by several factors: (i) length and quality of the available isotope and meteorological records, (ii) continuity of the records (only stations where it rains every month were considered), and (iii) different climatic regimes represented by the stations. For analysis of the long-term trends we selected 11 stations. Eight of them are located in Europe: four Swiss stations (Meiringen, Guttannen, and Grimsel, in a valley in the central Alps, and Bern, approximately 70 km to the northwest), Thonon-les-Bains (southern France, approximately 100 km southwest of Bern), Vienna (Austria), Groningen (the Netherlands), and Krakow (Poland). Data accumulated up to 1978 for the Swiss stations have been discussed by Siegenthaler and Oeschger (*28*). The remaining three stations are Ottawa (Canada), Hong Kong (United Kingdom), and Argentine Island (United Kingdom).

To determine the long-term relation between $\delta^{18}O$ and surface air temperature for the analyzed stations, we first removed the seasonal component from the available time series of monthly $\delta^{18}O$ and temperature by applying a 12-month running average. Then the departures, from the long-term means of $\delta^{18}O$ and temperature, $\Delta\delta^{18}O$ and ΔT, were calculated for individual stations. Finally, the resulting curves were smoothed by the application again of a 12-month running average. The composite trend curves for the Swiss stations and Europe (spatial averaging) were constructed by calculation of arithmetic averages of $\Delta\delta^{18}O$ and ΔT. This procedure is usually adopted for calculation of spatially averaged temperature records (*29*).

The trend curves of $\delta^{18}O$ for the Swiss stations (Fig. 2A) reveal a strong spatial coherence, indicating the presence of common mechanisms controlling long-term behavior of ^{18}O content in precipitation on this limited area. After 1986, $\delta^{18}O$ rose dramatically and reached a maximum of about 2 per mil above the 1970 to 1990 average toward the end of 1989. Interestingly, the $\delta^{18}O$ of spring water in the region closely followed this upward trend (*30*). The pronounced increase of $\delta^{18}O$ during recent years is evident also for other European stations, although spatial coherence among the individual trend curves decreases (Fig. 2B). The $\delta^{18}O$ trend curve for Thonon-les-Bains (not shown in Fig. 2B) closely follows the composite curve for Swiss stations.

In Europe, the calculated long-term changes of $\delta^{18}O$ and surface air temperature generally reveal strong temporal coherence. The composite curve of temperature changes for the Swiss stations indicates an apparent warming by ~1.5°C between 1986 and 1989 with respect to the 1970 to 1990 average. An analogous trend is also visible in the composite curve representing all European stations (Fig. 3A). The relation between $\delta^{18}O$ and temperature is different for other analyzed stations. The Hong Kong data, representing a tropical, monsoon-type

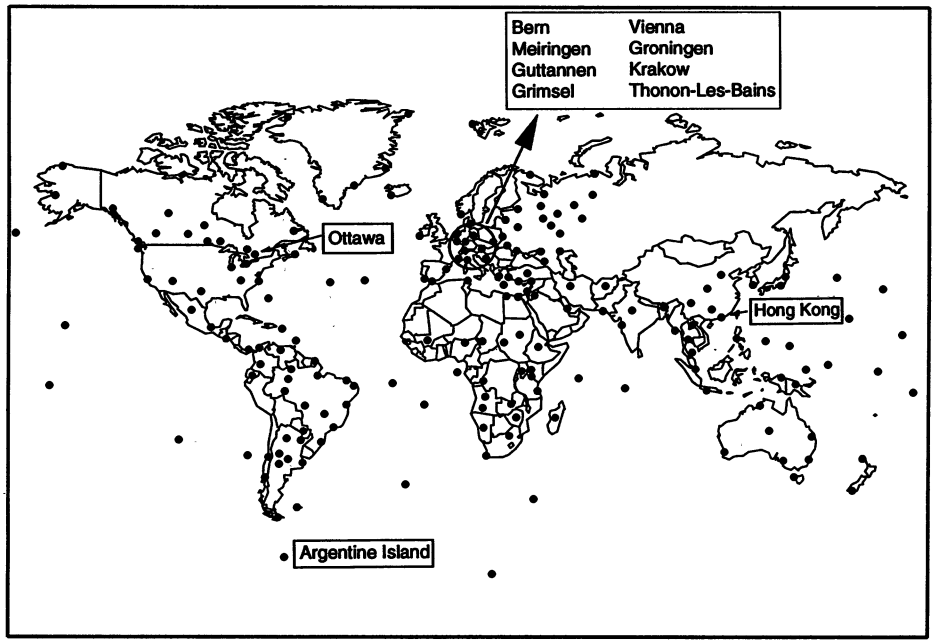

Fig. 1. The IAEA/WMO global network of stations collecting monthly precipitation samples for isotope analysis (only the stations for which a minimum of 3 years of stable isotope record is available are shown). The stations in this report for which long-term trends of $\delta^{18}O$ and surface air temperature were analyzed are identified by name.

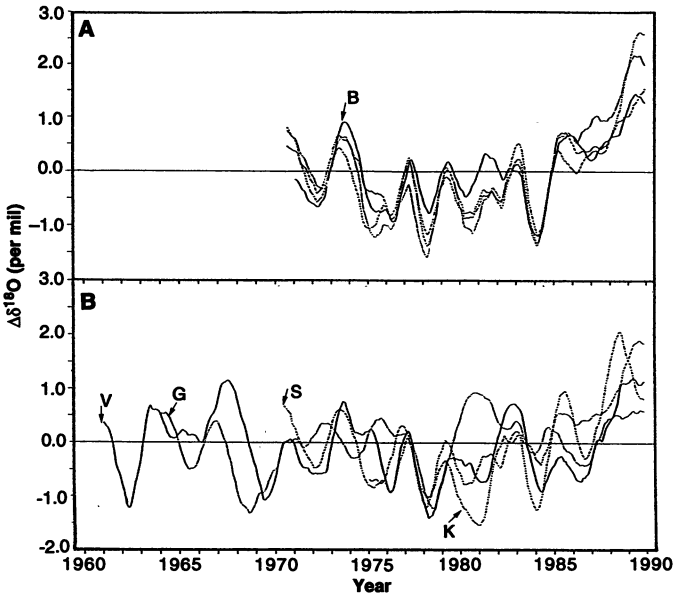

Fig. 2. Long-term trends of ^{18}O content in precipitation for selected European stations of the IAEA/WMO global network. (**A**) Trend curves of $\delta^{18}O$ calculated for four stations located in Switzerland: Meiringen, Guttannen, and Grimsel, in a valley in the central Alps and Bern, approximately 70 km northwest of the valley. Degree of spatial coherence between the trend curve for Bern (B) and the remaining three stations ranges from $r^2 = 0.85$ to 0.88, where r is the correlation coefficient. (**B**) Composite trend curve of $\delta^{18}O$ for the Swiss stations (S) ($r^2 = 0.71$) compared with three low-altitude European stations: Vienna, Austria (V); considered as a reference station; Groningen, the Netherlands (G) ($r^2 = 0.32$); and Krakow, Poland (K) ($r^2 = 0.69$).

climate, show relatively small fluctuations of both variables without apparent relation between them (Fig. 3C). Data from 1987 onward are not available. Weak temporal coherence between $\delta^{18}O$ and temperature variations was observed for Ottawa (Fig. 3B). There is no clear warming trend in recent years for this station. Argentine Island, in a high latitude of the Southern Hemisphere, reveals the strongest link between ^{18}O and temperature among the stations analyzed (Table 1). A distinct maximum around 1985 of both $\delta^{18}O$ and temperature was observed at this station (Fig. 3D). Data from 1987 onward are not available.

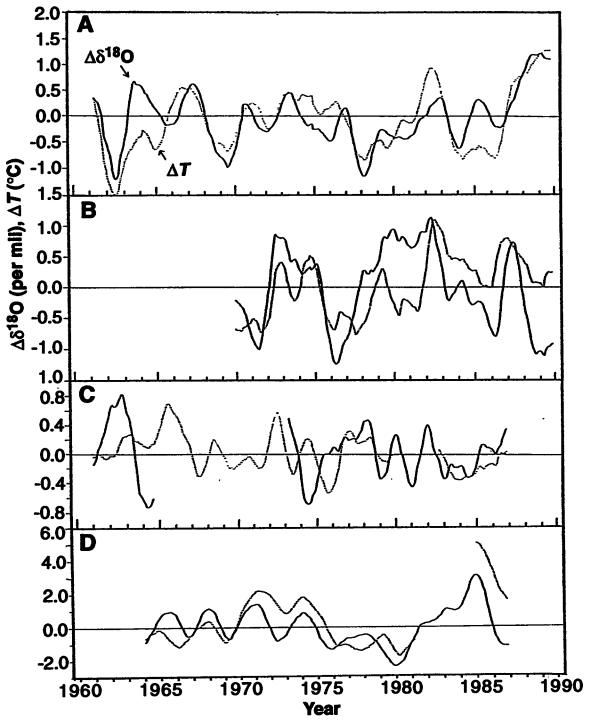

Fig. 3. Long-term trends of ^{18}O content in precipitation and surface air temperature for selected stations of the IAEA/WMO global network. (**A**) European stations, composite curves, (**B**) Ottawa, (**C**) Hong Kong, and (**D**) Argentine Island.

Three different types of $\delta^{18}O$-temperature relations, representing present climatic conditions, can be derived from the IAEA/WMO database: (i) a spatial relation between the long-term (annual) averages of $\delta^{18}O$ of precipitation and surface air temperature for different stations, (ii) a temporal relation between short-term (seasonal) changes of $\delta^{18}O$ and temperature for a single station or group of stations, and (iii) a temporal relation between long-term (interannual) changes of $\delta^{18}O$ and temperature for a fixed location.

The slope of relation (i) varies from Dansgaard's value of about 0.7 per mil per degree Celsius for high-latitude areas to virtually zero for tropical regions, where a strong relation between $\delta^{18}O$ and the amount of precipitation is usually observed (*2*, *6*). A slope as high as 0.90 per mil per degree Celsius was reported for the Antarctic Peninsula (*31*). For European stations in the IAEA/WMO network, the slope reaches 0.59 per mil per degree Celsius (Fig. 4A).

The seasonal $\delta^{18}O$-temperature coefficients derived from the monthly data for

Table 1. Seasonal and long-term $\delta^{18}O$-temperature coefficients for selected stations of the IAEA/WMO global network, "Isotopes in Precipitation." Periods in parentheses indicate length of the available $\delta^{18}O$ records. The long-term averages of temperature ($\overline{T}$), yearly precipitation ($\overline{P}$), and $\overline{\delta^{18}O}$ are listed for each station. In parentheses, weighted averages of $\delta^{18}O$ are indicated (weighing by amount of precipitation); *r* stands for correlation coefficient. Elevations are in meters above sea level.

Station	$\overline{T}$ (°C)	$\overline{P}$ (mm)	$\overline{\delta^{18}O}$ (per mil)	Seasonal $\Delta\delta^{18}O/\Delta T$ (per mil per degree Celsius)	r^2	Long-term $\Delta\delta^{18}O/\Delta T$ (per mil per degree Celsius)	r^2
Bern (1971 to 1990) 46.92°N, 7.50°E; 511 m	8.5	1090	−10.39 (−10.25)	0.33 ± 0.03	0.95	0.45 ± 0.07	0.17
Meiringen (1970 to 1990) 46.73°N, 8.20°E; 632 m	7.9	1321	−12.25 (−11.71)	0.50 ± 0.04	0.93	1.10 ± 0.10	0.35
Guttannen (1970 to 1990) 46.65°N, 8.30°E; 1055 m	6.2	1739	−13.03 (−12.82)	0.54 ± 0.03	0.96	0.87 ± 0.08	0.31
Grimsel (1970 to 1990) 46.57°N, 8.33°E; 1950 m	1.3	2149	−14.18 (−14.64)	0.45 ± 0.04	0.92	0.65 ± 0.05	0.41
Swiss stations (composite curves)						0.93 ± 0.07	0.41
Thonon-les-Bains (1963 to 1990) 46.22°N, 6.28°E; 385 m	10.2	982	−9.58 (−9.67)	0.36 ± 0.02	0.97	0.65 ± 0.07	0.20
Vienna (1961 to 1990) 48.25°N, 16.30°E; 203 m	9.9	610	−9.81 (−9.89)	0.39 ± 0.02	0.98	0.65 ± 0.05	0.36
Groningen (1964 to 1990) 53.21°N, 6.57°E; 0 m	9.6	751	−7.70 (−7.83)	0.23 ± 0.02	0.93	0.48 ± 0.04	0.30
Krakow (1975 to 1990) 50.07°N, 19.80°E; 205 m	7.7	619	−10.07 (−9.35)	0.34 ± 0.02	0.95	0.61 ± 0.07	0.30
Europe (composite curves)						0.63 ± 0.04	0.44
Ottawa (1970 to 1990) 45.32°N, 75.60°W; 114 m	5.8	884	−11.11 (−10.98)	0.31 ± 0.02	0.94	0.49 ± 0.08	0.14
Hong Kong (1961 to 1965) (1973 to 1987) 22.32°N, 114.10°E; 65 m	22.9	2219	−4.89 (−6.65)	−0.42 ± 0.04	0.91	0.25 ± 0.13	0.02
Argentine Island (1965 to 1987) 65.25°S, 64.20°W; 0 m	−4.1	377	−10.53 (−10.93)	0.31 ± 0.03	0.89	0.61 ± 0.05	0.40

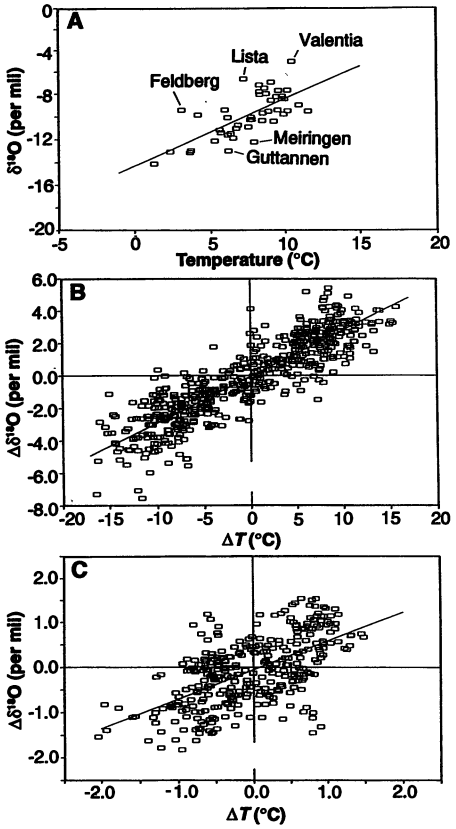

Fig. 4. Different types of $\delta^{18}O$-temperature relations for European stations of the IAEA/WMO global network. (**A**) Relation between the long-term annual averages of $\delta^{18}O$ and temperature for 47 stations in Europe. Both arithmetic ($\delta^{18}O_a$) and weighted ($\delta^{18}O_w$) averages were used to calculate the regression equations [$\delta^{18}O_a = (0.59 \pm 0.09)T - 14.35$, $r^2 = 0.49$; $\delta^{18}O_w = (0.59 \pm 0.08)T - 14.24$, $r^2 = 0.54$, weighing by amount of precipitation]. (**B**) Relation between departures of the long-term monthly means from the long-term annual means of $\delta^{18}O$ and temperature for 47 stations in Europe [$\Delta\delta^{18}O = (0.28 \pm 0.01)\Delta T - 0.07$, $r^2 = 0.78$]. Note the substantially lower slope of the regression line than that in (A). (**C**) Relation between the long-term trend curves of $\delta^{18}O$ and temperature for the Vienna station, which has the longest $\delta^{18}O$ record among the stations of the network [$\Delta\delta^{18}O = (0.65 \pm 0.05)\Delta T - 0.06$, $r^2 = 0.36$].

the individual stations [relation (ii)] appear substantially smaller than those derived from long-term trend curves of $\delta^{18}O$ and temperature (Table 1 and Fig. 4B) and the spatial relations of type (i). It has been argued that the $\delta^{18}O$-temperature coefficients derived from seasonal cycles of $\delta^{18}O$ and temperature for mid- and high-latitude stations might be useful for paleoclimatic applications because they cover a wide range of different "climates" (*16, 22, 28*).

The relation between long-term (interannual) changes of $\delta^{18}O$ in precipitation and surface air temperature for a given location seems to be the most appropriate as far as it concerns paleoclimatic reconstructions based on isotope records. Siegenthaler and Matter (*22*) investigated this relation for selected stations of mid- and high latitudes and found that the slope was significantly different from zero for only 4 out of 14 stations. However, the length of the analyzed records was rather short at that time (between 8 and 13 years). We calculated long-term $\delta^{18}O$-temperature coefficients, comparing the trend curves for individual stations and groups of stations (Table 1). Interestingly, the slopes appear substantially higher for data from the mountainous environments (Swiss stations) than for data from other European regions.

A recent study was conducted of stable isotope composition and noble gas content of ground waters in the Great Hungarian Plain, central Europe (*18*). It provides an opportunity to check paleoclimatic relevance of the $\delta^{18}O$-temperature coefficients derived from long-term changes of $\delta^{18}O$ in precipitation and temperature at a given location. The apparent $\Delta\delta^{18}O$ of ground waters in the region during the transition from Late Glacial to Holocene amounts to about 2.6 per mil. Similar enrichment in ^{18}O at this climatic boundary has been observed in carbonate sediments of several European lakes (*13–15*). The deuterium content of tree cellulose (German pine tree–ring chronology covering the Late Glacial–Holocene transition) also suggest that there was a similar change of ^{18}O in local ground water (*21*). The corresponding change of surface air temperature derived from the noble gas content of Hungarian ground waters is 7°C. Thus, the resulting apparent $\delta^{18}O$-temperature coefficient is about 0.37 per mil per degree Celsius. This value must be corrected for a $\Delta\delta^{18}O$ of the ocean during the Late Glacial–Holocene transition [~1.5 per mil according to Shackleton (*32*)]. The corrected slope is 0.59 per mil per degree Celsius, remarkably close to the value derived from long-term changes of $\delta^{18}O$ in precipitation and surface air temperature in Europe (0.63 ± 0.04 per mil per degree Celsius).

Validity of the $\delta^{18}O$-temperature coefficient derived from the trend curves of ^{18}O in precipitation and temperature can be also demonstrated on a shorter time scale. The coefficient for data from Argentine Island (0.61 ± 0.05 per mil per degree Celsius) agrees with an independent estimate based on isotope measurements of snow core collected at Dalinger Dome (Antarctic Peninsula), ~200 km northeast of this station (*33*). Comparison of δD variations measured in this core (between 1953 and 1980), with instrumental records of surface air temperature available for this region, leads to the δD-temperature coefficient of about 4.5 per mil per degree Celsius, corresponding to 0.56 per mil per degree Celsius for ^{18}O.

The presented data indicate that long-term changes of ^{18}O content in precipitation over mid- and high-latitude regions during the past three decades closely followed long-term changes of surface air temperature, thus confirming the importance of ^{18}O as a paleoclimatic indicator. An apparent warming trend observed over the past several years in Europe is reflected by enhanced $^{18}O/^{16}O$ isotope ratios of precipitation during this period. Interestingly, the isotopic composition of precipitation over mountainous regions seems to be more sensitive to long-term fluctuations of temperature than in low-altitude areas. It should be emphasized that the isotope signature of precipitation over mid- and high-latitude regions is controlled mainly by regional-scale processes [for example, conditions at the source regions of vapor, transport patterns of vapor in the atmosphere, average "rain-out history" of the air masses precipitating at a given place, and cloud-base temperature (*12, 26, 34*)]. Therefore, it should not be affected by local, surface phenomena such as "heat islands," although local temperature records often are. The $\delta^{18}O$-temperature coefficients derived from analysis of long-term trends in available records of ^{18}O in precipitation and surface air temperature agree well with independent estimates of these coefficients, derived from stable isotope and noble gas studies of ground waters as well as isotope analyses of contemporary snow deposits.

REFERENCES AND NOTES

1. H. Craig, *Science* **133**, 1702 (1961). The notation $\delta^{18}O = [(^{18}O/^{16}O)_S/(\text{sup18O}/^{16}O)_{SMOW} - 1] \times 1000$, where SMOW is standard mean ocean water and S is sample.
2. W. Dansgaard, *Tellus* **16**, 436 (1964).
3. I. Friedman, A. Redfield, B. Schoen, J. Harris, *Rev. Geophys.* **2**, 177 (1964).
4. W. Dansgaard, S. J. Johnsen, H. B. Clausen, N. Gundestrup, *Medd. Groenl.* **197**, 1 (1973).
5. R. Gonfiantini, *Acta Amazonica* **15**, 121 (1985).
6. Y. Yurtsever and J. R. Gat, in *Stable Isotope Hydrology, Deuterium and Oxygen-18 in the Water Cycle*, J. R. Gat and R. Gonfiantini, Eds. (International Atomic Energy Agency, Vienna, 1981), pp. 103–139.
7. S. Epstein, R. P. Sharp, A. J. Gow, *Science* **168**, 1570 (1970).
8. W. Dansgaard *et al.*, *ibid.* **218**, 1273 (1982).
9. C. Lorius, L. Merlivat, J. Jouzel, M. Pourchet, *Nature* **280**, 644 (1979).
10. J. Jouzel *et al.*, *ibid.* **329**, 403 (1987).
11. J. Jouzel and L. Merlivat, *J. Geophys. Res.* **89**, 11,749 (1984).
12. S. J. Johnsen, W. Dansgaard, J. W. C. White, *Tellus* **41B**, 452 (1989).
13. U. Eicher and U. Siegenthaler, *Boreas* **5**, 109 (1976).
14. _____, S. Wegmüller, *Quat. Res. N.Y.* **15**, 160 (1981).
15. K. Rozanski *et al.*, in *The Last Deglaciation: Absolute and Radiocarbon Chronologies*, E. Bard and W. Broecker, Eds. (Springer-Verlag, Berlin, 1992), pp. 69–81.
16. K. Rozanski, *Chem. Geol.* **52**, 349 (1985).

17. I. J. Winograd, B. J. Szabo, T. B. Coplen, A. C. Riggs, P. T. Kolesar, *Science* **227**, 519 (1985).
18. M. Stute, thesis, University of Heidelberg (1989).
19. S. Epstein and C. Yapp, *Earth Planet. Sci. Lett.* **30**, 252 (1976).
20. J. Lipp *et al.*, *Tellus* **43B**, 322 (1991).
21. B. Becker, B. Kromer, P. Trimborn, *Nature* **353**, 647 (1991).
22. U. Siegenthaler and H. A. Matter, in *Palaeoclimates and Palaeowaters: A Collection of Environmental Isotope Studies*, International Atomic Energy Agency, Vienna, 25 to 28 November 1980 (International Atomic Energy Agency, Vienna, 1983), pp. 37–53.
23. C. M. Van der Straaten and W. G. Mook, in *ibid.*, pp. 53–67.
24. C. Covey and P. L. Haagenson, *J. Geophys. Res.* **89**, 4547 (1984).
25. H. Craig and L. Gordon, in *Stable Isotopes in Oceanographic Studies and Palaeotemperatures, Spoleto 1965*, E. Tongiorgi, Ed. (Consiglio Nazionale della Richerche, Pisa, 1965), pp. 9–130.
26. L. Merlivat and J. Jouzel, *J. Geophys. Res.* **84**, 5029 (1979).
27. "Environmental Isotope Data. World Survey of Isotope Concentration in Precipitation," *IAEA Tech. Rep. Ser. Nos. 96, 117, 129, 147, 165, 192, 226, 264, 311* (1969, 1970, 1971, 1973, 1975, 1979, 1983, 1986, 1990).
28. U. Siegenthaler and H. Oeschger, *Nature* **285**, 314 (1980).
29. J. Hansen and S. Lebedeff, *J. Geophys. Res.* **92**, 13,345 (1987).
30. U. Schotterer, H. Oeschger, U. Siegenthaler, W. Stichler, in *Proceedings of the International Symposium on Isotope Techniques in Water Resources Development 1991*, Vienna, 11 to 15 March 1991 (International Atomic Energy Agency, Vienna, 1992), pp. 715–720.
31. D. A. Peel, R. Mulvaney, B. M. Davison, *Ann. Glaciol.* **10**, 130 (1988).
32. N. J. Shackelton, *Quat. Sci. Rev.* **6**, 183 (1987).
33. A. J. Aristarain, J. Jouzel, M. Pourchet, *Clim. Change* **8**, 69 (1986).
34. K. Rozanski, C. Sonntag, K. O. Münnich, *Tellus* **34**, 142 (1982).
35. We thank U. Siegenthaler, W. G. Mook, and J. Grabczak for providing the most recent data (1988 to 1990) for the Swiss stations, Groningen and Krakow, respectively. U. Siegenthaler provided constructive comments on the early version of the manuscript. We also thank M. Dray for providing the data for Thonon-les-Bains from 1980 to 1990.

26 May 1992; accepted 4 August 1992

Reductase Activity Encoded by the *HM1* Disease Resistance Gene in Maize

Gurmukh S. Johal and Steven P. Briggs

The *HM1* gene in maize controls both race-specific resistance to the fungus *Cochliobolus carbonum* race 1 and expression of the NADPH (reduced form of nicotinamide adenine dinucleotide phosphate)-dependent HC toxin reductase (HCTR), which inactivates HC toxin, a cyclic tetrapeptide produced by the fungus to permit infection. Several *HM1* alleles were generated and cloned by transposon-induced mutagenesis. The sequence of wild-type *HM1* shares homology with dihydroflavonol-4-reductase genes from maize, petunia, and snapdragon. Sequence homology is greatest in the βαβ-dinucleotide binding fold that is conserved among NADPH- and NADH (reduced form of nicotinamide adenine dinucleotide)-dependent reductases and dehydrogenases. This indicates that *HM1* encodes HCTR.

Since the discovery of a race-specific compatibility factor known as HC-toxin (*1*), disease caused by *Cochliobolus carbonum* Nelson race 1 has been the subject of detailed study. The presence of HC toxin permits the fungus to infect certain genotypes of maize (*Zea mays* L.) that would otherwise be resistant. The dominant allele of *HM1* determines resistance to the fungus and reduced sensitivity to HC toxin. The structure of HC toxin is known (*2*), but its mode of action remains to be elucidated (*3*). An enzyme that inactivates HC-toxin has been identified in extracts from maize (*4*). The enzyme, HC toxin reductase (HCTR), is detectable only in extracts from resistant genotypes (*5*). These results raised the question: does *HM1* encode or act as a regulator of HCTR? In this report we describe cloning the *HM1* gene and present evidence that *HM1* encodes HCTR activity.

Department of Biotechnology Research, Pioneer Hi-Bred International, Inc., Johnston, IA 50131.

Mutant alleles of *HM1* recovered from *Mutator* element stocks (*6*) were characterized. To identify co-segregation between *HM1* and restriction fragments containing a transposable element, the segregating progeny were first classified [with the use of Southern (DNA) blots] according to which *HM1* alleles they had inherited. The blots were hybridized with probes for RFLP loci that flank the locus; *PIO200644* and *PIO200044* map 5 centimorgans (cM) proximal and distal to *HM1*, respectively (*7*). Progeny that inherited intact the 10-cM block of chromosome 1 containing the mutant allele were grouped together, as were progeny that inherited the alternative allele. Recombinants were discarded. The classes were compared with each other on a Southern blot hybridized with a transposable element probe (*8*). Restriction fragments that were common to progeny that inherited the mutant allele and absent from the rest were identified. This method established linkage between restriction fragments containing a transposable element and the 10-cM block that contains the genetic locus *HM1*.

Five mutant alleles (Table 1) were analyzed. The 3.2-kb *Mu1* fragment that co-segregated with *hm1-656::Mu1* (Fig. 1) was cloned (*9*) and used to prepare a probe (designated *656) from the DNA flanking the *Mu1* insertion. The probe was used to map the clone relative to the dominant wild-type allele *Hm1*; no recombinants were observed in 60 backcross progeny. Comparison with the *Hm1-B79* allele revealed that the *Mu1* element had created an Sst I site upon insertion into *Hm1-B79*. The *656 probe was next hybridized to DNA from four different homozygous mutants all derived from the inbred line, B79. The observation of polymorphisms showed that DNA rearrangements were concomitant with mutagenesis. Similar results were obtained with *hm1-1369::Mu3*, in which *Mu3* was found to have inserted only 5 bp from the site of *Mu1* insertion in *hm1-656::Mu1*. We cloned the *hm1-1062::dHbr* allele using *656 as a probe. We mapped restriction sites in both wild-type and mutant alleles and found one restriction fragment length polymorphism. In the mutant allele, that restriction fragment contained a 315-bp insertion (designated "defective Heartbreaker," *dHBr*) with the general characteristics of a transposable element (*10*).

The *Def(HM1)-1790* allele was not transmitted through the pollen and was only poorly transmitted through the egg, typical of a chromosomal deletion. Neither the *1369 nor the *656 probes hybridized

Table 1. Properties of *hm1* alleles.

Allele*	Mutant sector†	Progenitor allele	Insertion element
hm1-656::Mu1	2/253 e	***Hm1-B79***	*Mu1*
hm1-1369::Mu3	1/230 e	***Hm1-B79***	*Mu3*
hm1-1062::dHbr	2/483 t	***Hm1-B79***	*dHbr*
Def(HM1)-1790	1/345 e	***Hm1-B79***	Deletion
hm1-1040::dSpm	63/672 t	***Hm1-4Co63***	*dSpm*

**hm1-1040::dSpm* was recovered from *P-VV/P-WW Hm1-4Co63*, whereas the other alleles arose in selfed *Mutator* plants (*Mutator Mu² per se*) that were crossed with the hybrid tester (K61/Pr) (*19*). †e = ear sector; t = tassel sector; mutants arose in progeny of crosses between plants homozygous for *Hm1* and possessing an active transposable element system and plants that were homozygous for *hm1*.